Constraining fault constitutive behavior with slip and stress heterogeneity

B. T. Aagaard[1] and T. H. Heaton[2]

Received 10 October 2006; revised 5 November 2007; accepted 16 January 2008; published 8 April 2008.

[1] We study how enforcing self-consistency in the statistical properties of the preshear and postshear stress on a fault can be used to constrain fault constitutive behavior beyond that required to produce a desired spatial and temporal evolution of slip in a single event. We explore features of rupture dynamics that (1) lead to slip heterogeneity in earthquake ruptures and (2) maintain these conditions following rupture, so that the stress field is compatible with the generation of aftershocks and facilitates heterogeneous slip in subsequent events. Our three-dimensional finite element simulations of magnitude 7 events on a vertical, planar strike-slip fault show that the conditions that lead to slip heterogeneity remain in place after large events when the dynamic stress drop (initial shear stress) and breakdown work (fracture energy) are spatially heterogeneous. In these models the breakdown work is on the order of MJ/m^2, which is comparable to the radiated energy. These conditions producing slip heterogeneity also tend to produce narrower slip pulses independent of a slip rate dependence in the fault constitutive model. An alternative mechanism for generating these confined slip pulses appears to be fault constitutive models that have a stronger rate dependence, which also makes them difficult to implement in numerical models. We hypothesize that self-consistent ruptures could also be produced by very narrow slip pulses propagating in a self-sustaining heterogeneous stress field with breakdown work comparable to fracture energy estimates of kJ/M^2.

Citation: Aagaard, B. T., and T. H. Heaton (2008), Constraining fault constitutive behavior with slip and stress heterogeneity, *J. Geophys. Res.*, *113*, B04301, doi:10.1029/2006JB004793.

1. Introduction

[2] Uncovering the physics controlling earthquake rupture is an inherently difficult task because ruptures are relatively infrequent and hidden from direct observation several kilometers below the ground surface. Nevertheless, with current computational resources it is becoming much more common for researchers to strive to reproduce the dynamics of natural earthquakes. When attempting to tie models of earthquake rupture to natural behavior we must keep in mind that there is likely a range of model parameters that produces similar results and a model may capture only the most general physics of the rupture process. Understanding the ramifications of this second issue requires a thorough knowledge of the numerical limitations of a model and the range of physical processes capable of generating seismologic and geodetic observations.

[3] Current numerical models of spontaneous dynamic ruptures involve spatial and temporal discretizations of the model space, using techniques such as finite differences [e.g., *Andrews*, 1976a; *Day*, 1982], finite elements [e.g., *Mikumo and Miyatake*, 1978; *Oglesby et al.*, 1998; *Aagaard et al.*, 2001], or boundary integral techniques [e.g., *Lapusta et al.*, 2000]. As a result, the range of length scales, even with state-of-the-art supercomputers, is limited to a few orders of magnitude. Earthquake ruptures, on the other hand, are often associated with fractal distributions (e.g., Gutenberg-Richter frequency-magnitude relation and fractal spatial distributions of faults and earthquakes) [*Turcotte and Malamud*, 2002]. In terms of rupture behavior, one could infer from the fractal nature of earthquake behavior that slip occurs via slip pulses in small events in much the same fashion as it does in large events. In other words, the length scale of the slip pulse (i.e., the distance from the leading edge of the rupture to the trailing edge of the rupture at any given instant during the earthquake) could be several orders of magnitude smaller in size than the total rupture length.

[4] Very narrow, confined slip pulses would also be compatible with sudden changes in sliding friction from high static values (coefficient of friction, $\mu_f \approx 0.6$) to low dynamic values ($\mu_f < 0.1$) and back again. Faults would appear to be "strong" in the static sense but "weak" in the dynamic sense, solving the heat paradox associated with the absence of ubiquitous heat production on faults from earthquake ruptures [*Heaton*, 1990]. Fault constitutive models with a strong rate dependence produce such narrow slip pulses [e.g., *Cochard and Madariaga*, 1994]. Unfortunately, they lead to ill-posed numerical solutions, either due to the absence of a breakdown zone (for the case of pure rate-dependent friction) or a breakdown zone much smaller

[1]U.S. Geological Survey, Menlo Park, California, USA.
[2]Department of Geologic and Planetary Sciences, California Institute of Technology, Pasadena, California, USA.

0148-0227/08/2006JB004793$09.00

than what can be resolved with current discretization schemes [*Rice*, 1993; *Madariaga and Cochard*, 1994]. For example, friction stress changes occurring over a few milliseconds (which, for the linear slip-weakening friction model, correspond to values of slip-weakening parameter in the range of a few millimeters) require discretization sizes on the order of a few meters, which is nearly 2 orders of magnitude smaller than what most current three-dimensional (3-D) numerical models of spontaneous rupture use. Thus, our current numerical models do not span a sufficient range of length scales to simultaneously capture these very short length scales while still capturing the large-scale 3-D effects of fault slip and rupture propagation.

[5] One possible mechanism for working around this difficult issue of capturing the vast range of length scales involved in dynamic ruptures is to assume that we can encapsulate small length-scale behavior within the fault constitutive model, thereby permitting use of a numerical simulation that spans only a subset of the length scales that may be involved. We can also use such simulations to guide our inferences in the behavior across a broader range of scales. Keeping these limitations of the numerical models in mind and our desire to ultimately make inferences about the behavior across a broader range of scales, we now focus on trying to understand the constraints on fault constitutive models in spontaneous dynamic ruptures simulations.

[6] Researchers often attempt to constrain their spontaneous rupture models by matching strong ground motion records or the rupture propagation imaged in kinematic source inversions. Unfortunately, these provide only the most basic constraints on stress drop and breakdown work or fracture energy [see, e.g., *Guatteri and Spudich*, 2000; *Peyrat et al.*, 2001; *Mikumo et al.*, 2003; *Zhang et al.*, 2003; *Peyrat et al.*, 2004]. In some cases [e.g., *Guatteri and Spudich*, 1998] these techniques have been used to constrain the absolute level of shear stress, but in most cases the modeler selects the absolute level of shear stress arbitrarily.

[7] On the other hand, the spectral characteristics of slip appear to be better constrained [*Somerville et al.*, 1999; *Mai and Beroza*, 2002; *Lavallée and Archuleta*, 2003; *Liu-Zeng et al.*, 2005]. The fractal nature of the slip appears to be associated with other scaling relationships as well, such as the ratio of slip to rupture length and average stress drop [*Liu-Zeng et al.*, 2005]. Several recent studies of spontaneous dynamic rupture have tried to exploit this to examine the physics of the rupture, including how variations in slip, risetime, and rupture speed affect near-source ground motions [*Oglesby and Day*, 2002; *Guatteri et al.*, 2003] and whether a contrast in elastic properties across a fault affects rupture propagation in the presence of a heterogeneous stress field [*Andrews and Harris*, 2005]. In generating the appropriate spatial-temporal evolution of slip, there is often a trade-off between influencing the slip via spatial variations in initial stress and spatial variations in the fault constitutive properties [*Peyrat et al.*, 2004].

[8] *Peyrat et al.* [2004] found that they could match strong motion records along with GPS and InSAR measurements of ground deformation equally well with either (1) a spatially heterogeneous distribution of initial shear stress and spatially homogeneous fault constitutive parameters or (2) a spatially homogeneous distribution of initial shear stress and spatially heterogeneous fault constitutive parameters. Whereas ruptures were nearly identical from the view of seismologic and geodetic observations (the ground motions and static displacements they produced) the different fault constitutive parameterizations imply the physics controlling the ruptures were quite different. Furthermore, the postrupture shear stress fields over the rupture area were diametrically opposite of each other. In the case of the initially heterogeneous shear stress field, the postrupture shear stress field was rather homogeneous, whereas in the case of the initially homogeneous shear stress field, the postrupture shear stress field was quite heterogeneous. In other words, in one case the stress field went from heterogeneous to homogeneous, and in the other case it went from homogeneous to heterogeneous. One expects that natural faults operate somewhere between these two extremes [*Rivera and Kanamori*, 2002].

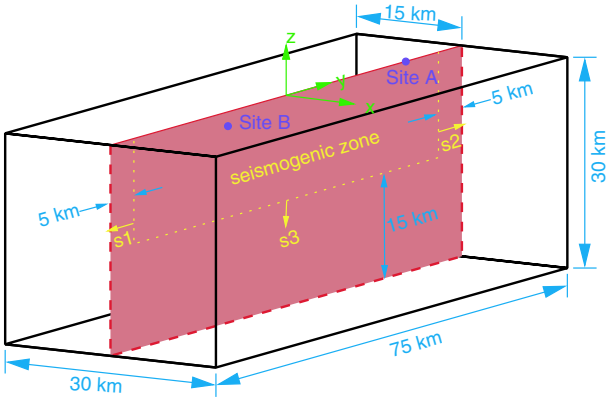

Figure 1. Geometry of the vertical strike-slip fault and simulation domain. The random spatial variations are tapered outside of the seismogenic zone using equation (9), where s is s_1, s_2, or s_3. We compare velocity time histories at sites A (x = 0 km, y = 26 km) and B (x = 5 km, y = −20 km).

[9] In this study, we attempt to find sets of parameters conducive to this self-consistent behavior associated with faults operating between the two extremes of (1) ruptures removing all heterogeneity from the shear stress field and (2) ruptures introducing all heterogeneity into the shear stress field. Heterogeneous final slip in an earthquake corresponds to spatial variations in the static stress drop. These spatial variations in stress drop likely develop because both the prerupture shear stress field and the fault friction are spatially heterogeneous. Using spontaneous dynamic rupture simulations with different combinations of initial conditions and fault friction parameters we try to produce ruptures with heterogeneous slip and similar slip time histories. We then judge whether the conditions following a rupture are consistent with those preceding rupture. In this way we seek to find additional constraints on the parameters in spontaneous rupture simulations beyond those necessary to produce a given spatial-temporal evolution of slip.

2. Methodology

[10] We study spontaneous dynamic rupture propagation on a vertical, throughgoing strike-slip fault that is embedded in a 75 km long, 30 km wide, and 30 km deep domain as shown in Figure 1. Table 1 lists the principal parameters

Table 1. Description of Parameters

Parameter	Description
σ_f	Friction stress
σ_{fail}	Failure stress
$\sigma_{sliding}$	Sliding friction stress
σ_0	Initial stress
τ_{xy}	Stress tensor component xy
λ, μ	Lame's constants
$D(t)$	Slip at a point on the fault
$\dot{D}(t)$	Slip rate at a point on the fault
D_0	Slip-weakening parameter in fault constitutive model
V_0	Restrengthening threshold in fault constitutive model
$C(t)$	Restrengthening parameter in fault constitutive model
$\delta(t)$	State variable in fault constitutive model
$\dot{\delta}(t)$	Rate of change in state variable
$\dot{\delta}_{\max}$	Maximum rate of change in state variable
$\dot{\delta}_r$	Rate of restrengthening in fault constitutive model
κ	Rupture propagation parameter, see equation (10)
L	Length scale related to rupture width, see equation (10)
W_b	Breakdown work
κ^*	Nominal value of κ
α_{dyn}	Fraction of perturbation in κ accounted for by perturbations in dynamic stress drop
α_{fail}	Fraction of perturbation in breakdown work accounted for by perturbations in failure s tress relative to sliding friction stress

used in this study. In order to create ruptures with some of the basic features present in natural earthquakes, we include variation in the material properties with depth and overburden pressure (hydrostatic pore pressures). The material properties follow horizontally averaged values of v_p, v_s, and density (given in Table 2 and Figure 2) from the Southern California Earthquake Center Community Velocity Model [*Magistrale et al.*, 2000]. We normalize stress related fault constitutive model parameters with respect to the shear modulus, which gives rise to behavior that is similar to using a homogeneous half-space. We use the same spontaneous dynamic rupture finite element code as we have used in previous studies [e.g., *Aagaard et al.*, 2001, 2004]; in benchmark tests [*Harris and Archuleta*, 2004] it gives very similar results to several other finite element and finite difference spontaneous rupture codes. We discretize the domain using linear tetrahedral finite elements with the length of element edges set to approximately one tenth of the wavelength of shear waves with periods of 1.0 s. The elements at the bottom of the domain have 375 m long edges whereas the elements at the top of the domain have 265 m long edges (very similar results were obtained for simulations with elements twice these sizes). This discretization resolves fault rupture associated with wave propagation at periods of 1.0 s and longer.

[11] Numerous fault constitutive models have been proposed to describe various aspects of slip on faults associated with earthquake rupture. Some, such as rate and state friction [e.g., *Dieterich*, 1979], are derived directly from laboratory measurements. Others, such as slip weakening [e.g., *Ida*, 1972], are used primarily because they are simple and promote numerical stability. More recently, *Ohnaka* [2003] proposed a slip-based fault constitutive model that encapsulates both laboratory observations and simple scaling relationships. Alternatively, *Rice* [2006] proposed that field observations of thin primary slip surfaces and a lack of widespread melting in fault cores imply thermal processes (thermal pressurization and flash heating) may control weakening with the onset of slip in earthquake rupture. Other fault constitutive models, such as time weakening [*Andrews*, 2004], are variations of theoretical (in this case, slip weakening) or laboratory-based models that provide greater numerical stability for use in spontaneous rupture simulations. In this study, we use a simple fault constitutive model that blends the classic slip-weakening friction model with the restrengthening present in slip-plus-rate-weakening friction, while including some additional features to ensure its numerical stability. However, it is important to recognize that choosing fault constitutive models that promote numerical stability could potentially remove important physics that occur in real earthquakes.

[12] Both slip-weakening and slip-plus-rate-weakening friction models are widely used fault constitutive models in spontaneous dynamic rupture modeling [see, e.g., *Harris*, 2004, and references therein]. In slip-plus-rate-weakening models friction increases (the fault restrengthens) as slip rate decreases, whereas in slip-weakening models friction usually remains at the sliding friction level even after sliding stops (no restrengthening occurs). In contrast, rate and state friction models include an increase in friction with the logarithm of the time once sliding stops. A simple way to incorporate restrengthening in slip-weakening models is to impose instantaneous restrengthening wherein the strength returns to its presliding level immediately upon the termination of slip [see, e.g., *Aagaard et al.*, 2001]. However, this abrupt restrengthening often increases numerical noise in the simulations through sudden stops and restarts in sliding.

[13] In order to generate a continuous spectrum of shear restrengthening behavior, we develop a common parameterization for slip weakening with and without restrengthening. Other studies [*Madariaga and Cochard*, 1994; *Shaw*, 1995; *Nielsen et al.*, 2000] have also blended slip-weakening and slip-plus-rate-weakening friction models using various formulations. We introduce a state variable, δ, to add restrengthening to the linear slip-weakening friction model yielding

$$\sigma_f = \left(\sigma_{fail} - \sigma_{sliding}\right)\left(1 - \frac{\delta(t)}{D_0}\right) + \sigma_{sliding},$$
$$\dot{\delta}(t) = \dot{D}(t) - C(t) \tag{1}$$

$$C(t) = \begin{cases} \dot{\delta}_r, \text{ if } \dot{D}(t) \le V_o \ \ \& \ \ \ddot{D}(t) \le 0 \\ 0, \text{ otherwise} \end{cases}$$
$$\dot{\delta}(t) \le \dot{\delta}_{\max}, \ 0 \le \delta(t) \le D_0, \tag{2}$$

Table 2. Material Properties[a]

Depth (km)	Mass Density (kg/m^3)	Dilatational Wave Speed (km/s)	Shear Wave Speed (km/s)
0	2600	5.70	3.40
11.0	2800	6.30	3.60
22.0	3000	6.90	3.85
38.0	2300	7.80	4.50
40.0	3300	7.80	4.50

[a]Control points describing the piecewise linear variation of material properties with depth.

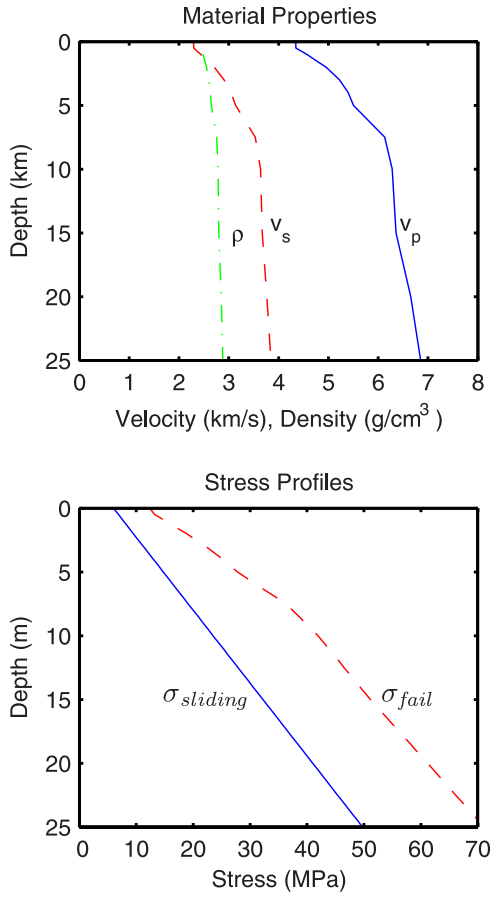

Figure 2. (top) Material properties and (bottom) fault constitutive properties as a function of depth. The shear wave speed (v_s), dilatational wave speed (v_p), and mass density (ρ) define the material properties. The sliding stress ($\sigma_{sliding}$) increases linearly with depth, and the failure stress (σ_{fail}) varies with the shear modulus.

where σ_f denotes the friction stress, σ_{fail} denotes the failure stress, $\sigma_{sliding}$ denotes the sliding friction stress, D denotes slip, D_0 denotes the slip-weakening parameter, and $\dot{\delta}_r$, V_0, and $\dot{\delta}_{\max}$ are other parameters (see Table 1). Figure 3 shows a typical trajectory of the friction stress in slip and slip rate space. We choose to specify the friction explicitly in terms of stresses and independent of the fault normal stress, because dynamic changes in friction during slip may be independent of the overburden pressure as a result of dynamic processes [see, e.g., *Brune et al.*, 1993; *Melosh*, 1996; *Tworzydlo and Hamzeh*, 1997; *Brodsky and Kanamori*, 2001].

[14] Traditional slip weakening behavior with no restrengthening is produced by setting $\dot{\delta}_r = 0$. This results in $C = 0$ for all t and $\delta(t) = D(t)$ until $\delta(t) = D_0$ after which it is clipped to D_0. We also include elements of time-weakening friction [*Andrews*, 2004] to increase the numerical stability of the solution by limiting the maximum rate of decrease of the friction stress, $\dot{\delta}(t) \leq \dot{\delta}_{\max}$. This increases the size of the breakdown zone to several hundred meters for several meters of slip. This breakdown zone is 2 or more orders of magnitude larger than those in natural earthquakes if processes such as flash heating cause very rapid dynamic shear stress changes. In fact, rapid changes in dynamic friction necessarily imply small breakdown work. Thus, while we use a breakdown work comparable to radiated energy in our numerical model to promote numerical stability, we recognize that breakdown work could be much smaller and that the spatial distribution of prestress may largely control earthquake dynamics.

[15] For the restrengthening portion of the fault constitutive model, we employ a simple dependence on a slip rate threshold, V_0, and a rate of restrengthening, $\dot{\delta}_r$. If $\dot{\delta}_r$ is chosen to be nonzero (and positive), then when the slip is decelerating ($\ddot{D}(t) \leq 0$) and the slip rate is below some threshold (V_0), $C > 0$ and the state variable decreases toward zero. As a result, friction increases associated with restrengthening. If $V_0 = 0$, then restrengthening at a point occurs only after sliding terminates. This corresponds to traditional slip-weakening behavior during sliding but the fault restrengthens at a constant rate when sliding stops; this is somewhat faster than the logarithmic time dependence found in rate and state friction [e.g., *Dieterich*, 1979]. On the other hand, if $V_0 > 0$, then restrengthening occurs while the slip rate is greater than zero producing rate-activated restrengthening where $\dot{\delta}_r$ controls the rate of restrengthening. This formulation is slightly more stable numerically than a direct rate dependence (used in previous studies such as those by *Aagaard et al.* [2001] *Anderson et al.* [2003], and *Aagaard et al.* [2004]) because the rate of restrengthening is constant and does not increase as the slip rate decreases.

[16] We consider three levels of restrengthening: no restrengthening ($\dot{\delta}_r = 0$), slip weakening with restrengthening after sliding stops ($V_0 = 0$, $\dot{\delta}_r = 0.325$ m/s), and slip weakening with rate-activated restrengthening ($V_0 = 0.20$ m/s, $\dot{\delta}_r = 0.325$ m/s). For brevity, we will generally refer to these three cases as without restrengthening, restrengthening at rest, and rate-activated restrengthening. Table 3 summarizes the differences in friction model parameters for these three levels of restrengthening. In all three cases, we set $\dot{\delta}_{\max} = 2.0 D_0$/s so that it takes at least 0.5 s for the friction to drop from σ_{fail} to $\sigma_{sliding}$ and we can resolve the breakdown zone. The remaining two principal parameters of the fault constitutive model (σ_{fail} and D_0) will be included in the spatial variation of the parameters as discussed later.

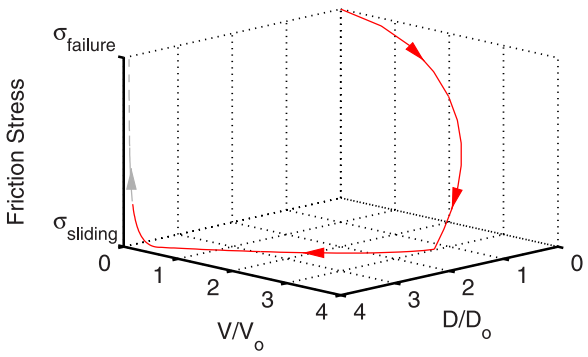

Figure 3. A typical trajectory of the friction stress in slip (D) and slip rate (V) space. The friction decreases in response to slip weakening and then increases as the slip rate drops below a threshold. The gray, dashed portion of the trajectory depicts the restrengthening after sliding stops.

Table 3. Friction Parameters for the Three Levels of Shear Restrengthening[a]

Scenario	$\dot{\delta}_r$ (m/s)	V_0 (m/s)
noR	0	0
restR	0.325	0
rateR	0.325	0.20

[a]The friction models noR, restR, and rateR refer to slip weakening without restrengthening, slip weakening with restrengthening at rest, and slip weakening with rate-activated restrengthening, respectively.

[17] We construct the prestress field by superposition of (1) a nominal background stress field, (2) a uniform shear strain field, and (3) a random strain field. The nominal background stress field,

$$\tau_{xy} = 6\,\mathrm{MPa} - 1.75\,\mathrm{MPa/km}\; z, \tag{3}$$

$$\tau_{xx} = 1.0 \times 10^{-4}\frac{4\mu(\lambda+\mu)}{\lambda+2\mu} + \int_0^z (\rho(s)-\rho_w)g\,ds, \tag{4}$$

$$\tau_{yy} = 1.0 \times 10^{-4}\frac{2\mu\lambda}{\lambda+2\mu} + \int_0^z (\rho(s)-\rho_w)g\,ds, \tag{5}$$

$$\tau_{zz} = \int_0^z (\rho(s)-\rho_w)g\,ds, \tag{6}$$

$$\tau_{yz} = \tau_{xz} = 0, \tag{7}$$

corresponds to linearly increasing shear stress with depth (z is positive upward), lithostatic overburden pressure (with hydrostatic pore pressure), and horizontal compression, where $\rho(z)$ denotes the density as a function of z, ρ_w denotes the density of water, g denotes the acceleration of gravity, and λ and μ denote Lame's constants. The shear stress increases with depth at a rate such that heat production associated with a 2 cm thick zone and 2 m of frictional sliding (excluding breakdown work or fracture energy) at a depth of 15 km will give rise to temperature changes less than 1200 K (using a heat capacity of per unit mass of 1000 J/(kg K)). This modest temperature increase is consistent with the lack of substantial melting found in some exhumed faults [*Chester and Chester*, 1998].

[18] The overburden pressure dominates the fault normal and fault parallel axial stresses (τ_{xx} and τ_{yy}) except near the surface. With compressive strains in the fault normal direction ($\epsilon_{xx} = 1.0 \times 10^{-4}$), we keep the fault in compression even under dynamic loading. As a result, the angle between the fault and the maximum principal stress direction is a little more than 45 degrees except at depths less than about a kilometer where the overburden pressure is not significantly larger than the fault normal compressive stress.

[19] On the basis of the characterization of slip heterogeneity by *Mai and Beroza* [2002] with von Karman distributions, we construct the random strain field by finding the strain field associated with a random slip field by solving the static elasticity equation in our model. The power spectra of the random slip follows a von Karman distribution,

$$P(k) = \frac{a_y a_z}{(1+k^2)^{(H+1)}}, \tag{8}$$

where k is the radial wave number ($k^2 = a_y^2 k_y^2 + a_z^2 k_z^2$), a_y = 20 km, a_z = 10 km, and H = 0.75. We build the slip distribution by starting with a normally distributed random field (zero mean with a variance of 1.0) in the wave number domain. The magnitude of the amplitude in the wave number domain is set to match the von Karman distribution. We prevent inclusion of short-length-scale features that the finite element model cannot resolve by setting the spectral components associated with wavelengths shorter than 5.0 km to zero. After transforming to the spatial domain, we taper the random distribution along the edges of the fault as shown in Figure 1. This approach is very similar to the one used by *Andrews and Harris* [2005]. The tapering limits the seismogenic zone to the top half of the domain and prevents ruptures from propagating to the lateral edges of the domain (where they would create edge effects not present in natural earthquakes). The taper follows an exponential variation,

$$f_{taper} = \begin{cases} 1 - \frac{1}{2}e^{3s/s_0} \text{ if } s < 0 \\ \frac{1}{2}e^{-3s/s_0} \text{ if } s \geq 0, \end{cases} \tag{9}$$

where s denotes distance from the center of the taper, and s_0 is the nominal taper width (5.0 km). The final step involves scaling the distribution by a factor of 150 to create the slip distribution used in the static simulation to calculate the random strain field on the fault surface.

[20] We want to produce similar slip time histories from different combinations of initial shear stress and fault constitutive parameters. Unfortunately, we do not have a general prescription for generating the initial conditions and fault constitutive model parameters required to produce a given spatial-temporal evolution of slip. Consequently, using trial and error we selected a set of uniform fault constitutive parameters and the spatially heterogeneous stress field described earlier to generate a magnitude 7.2 event that ruptures a sizable fraction of our fault (820 km^2). We use these parameters and rupture as our reference from which we construct other simulations with different initial conditions and fault constitutive parameters that yield similar rupture behavior.

[21] *Day* [1982] and *Madariaga and Olsen* [2000] found that a nondimensional parameter,

$$\kappa = \frac{(\sigma_0 - \sigma_{sliding})^2 L}{W_b \mu} \tag{10}$$

(σ_0 is the initial shear stress, $\sigma_{sliding}$ is the sliding friction, W_b is the breakdown work, μ is the shear modulus, and L is the width of the slip pulse), correlates with the extent and speed of rupture propagation. We follow *Tinti et al.* [2005] in using the term breakdown work instead of fracture energy, because we consider fault constitutive behavior at a macroscopic scale and do not distinguish among the various

Table 4. Parameters Associated With Nominal Value of κ[a]

L^*	1.00 km
W_b^*/μ	1.62×10^{-4}
D_0^*	0.65 m
$(\sigma_{fail}^* - \sigma_{sliding}^*)/\mu$	5.00×10^{-4}
$(\sigma_0^* - \sigma_{sliding}^*)/\mu$	1.76×10^{-4}

[a]With $\kappa^* = 0.19$. Note that the nominal sliding stress $\sigma_{sliding}^*$ is equal to the nominal background stress τ_{xy} (equation (3)).

mechanisms dissipating energy at the rupture front, e.g., creation of new surfaces (fracture energy), frictional sliding on secondary slip surfaces, and inelastic deformation in the surrounding volume. This nondimensional parameter is proportional to the inverse of the critical crack length required for rupture propagation [*Andrews*, 1976b; *Day*, 1982] and roughly approximates the ratio of the available strain energy ($W \approx (\sigma_0 - \sigma_{sliding})^2 L/\mu$) to the breakdown work (W_b) [*Madariaga and Olsen*, 2000]. If we replace the sliding friction with the final shear stress in the expression for κ this would be less of an approximation but we would not be able to compute κ prior to rupture. Although κ is formulated in the context of a homogeneous half-space with uniform initial shear stresses and fault constitutive model parameters, it provides a convenient parameter related to macroscopic rupture behavior (rupture extent and rupture speed) that we can keep constant across our suite of simulations. Other parameters, such as dynamic stress drop and relative strength $S = (\sigma_{fail} - \sigma_0)/(\sigma_0 - \sigma_{sliding})$ [*Andrews*, 1976a]), display a greater dependence on the details of the fault constitutive model for a given spatial-temporal evolution of slip than κ.

[22] We construct the common baseline for our suite of spontaneous rupture simulations by computing κ on the fault surface for our reference magnitude 7.2 event. We also compute a nominal, uniform κ^*, such that κ/κ^* describes the perturbation in the initial conditions and fault constitutive parameters from some nominal, uniform state. If we arbitrarily select $L = 1$ km (because L loses its original ties to rupture width in our heterogeneous setting), then $\kappa = 0.19$ corresponds to our nominal, uniform value; we denote the associated nominal values for the initial shear stress, sliding friction, and breakdown work by σ_0^*, $\sigma_{sliding}^*$, and W_b^*, where $\kappa^* = (\sigma_0^* - \sigma_{sliding}^*)^2/(W_b^* \mu)$ as expected. Table 4 gives the nominal values of the parameters associated with κ^* in our simulations. This nominal value, κ^*, is the "average" over the entire fault surface; the ruptures will preferentially propagate over the area in which κ is locally high, so the average over the area where slip occurs will be considerably higher than 0.19.

[23] We construct our suite of spontaneous rupture simulations with variations in the spatial distributions of the initial shear stress and fault constitutive parameters by associating these variations in the parameters with the spatial variation in κ (see Figures 4–6 top) relative to κ^*. This provides a systematic way of considering a continuous range of trade-offs among the dynamic stress drop (initial shear stress) and fault constitutive parameters (e.g., breakdown work, slip-weakening parameter, and failure stress).

[24] The random strain field used to construct the spatial variation in κ contains nonzero tractions in both the along-strike and updip directions. However, κ is a scalar, so it does not contain information about the perturbations in the orientation of the initial stress field; consequently, we simply apply the shear stresses in the horizontal direction, which is consistent with the strike-slip faulting. We allow rake rotations so the slip is not constrained to be in the horizontal direction.

[25] Examining the expression for κ, one recognizes that mapping perturbations in κ results in examining trade-offs between perturbations in dynamic stress drop ($\sigma_0 - \sigma_{sliding}$) and breakdown work ($W_b$). In our parameterization breakdown work is characterized by the failure stress ($\sigma_{fail} - \sigma_{sliding}$) and the slip-weakening parameter (D_0). Appendix A explains how we relate perturbations in κ to perturbations in the initial shear stress, failure stress, and slip-weakening parameter using nondimensional parameters α_{dyn} and α_{fail}. α_{dyn} specifies the fraction of the perturbation in κ that arises from perturbations in the dynamic stress drop, and α_{fail} specifies the fraction of the perturbation in the breakdown work that arises from perturbations in the failure stress. This yields

$$\frac{\sigma_0 - \sigma_{sliding}}{\mu} = \left(\frac{\sigma_0^* - \sigma_{sliding}^*}{\mu}\right)\left(\frac{\kappa}{\kappa^*}\right)^{\frac{\alpha_{dyn}}{2}} \tag{11}$$

for the initial stress field relative to the sliding stress (dynamic stress drop),

$$\frac{\sigma_{fail} - \sigma_{sliding}}{\mu} = \left(\frac{\sigma_{fail}^* - \sigma_{sliding}^*}{\mu}\right)\left(\frac{\kappa}{\kappa^*}\right)^{\alpha_{fail}\left(\alpha_{dyn}-1\right)} \tag{12}$$

for the failure stress relative to the sliding friction stress, and

$$D_0 = D_0^*\left(\frac{\kappa}{\kappa^*}\right)^{\left(1-\alpha_{fail}\right)\left(\alpha_{dyn}-1\right)} \tag{13}$$

for the slip-weakening parameter, where α_{dyn} and α_{fail} can be between 0 and 1, inclusively. When $\alpha_{dyn} = 1$, spatial variations in κ arise exclusively from spatial variations in dynamic stress drop; alternatively, when $\alpha_{dyn} = 0$, spatial variations in κ arise exclusively from spatial variations in breakdown work. Similarly, when $\alpha_{fail} = 1$, spatial variations in breakdown work arise exclusively from spatial variations in the failure stress relative to the sliding friction stress, whereas when $\alpha_{fail} = 0$, spatial variations in breakdown work arise exclusively from spatial variations in the slip-weakening parameter, D_o.

[26] In this study we focus on the spatial variability of the initial and final shear stress relative to the sliding friction stress, rather than the spatial variability in the absolute level of the stress. For our sets of parameters, including spatial variations in the sliding friction, while keeping the initial and failure stress relative to the sliding friction the same, does not change the spatial and temporal evolution of slip. Furthermore, we will use these relative stresses to judge the preearthquake and postearthquake consistency in the spatial heterogeneity of the stress field. Consequently, we do not consider spatial variations in the sliding friction: we map spatial variations in the dynamic stress drop into spatial variations in the initial shear stress, and spatial variations in the failure stress relative to the sliding friction directly into the failure stress, keeping the sliding friction stress equal to

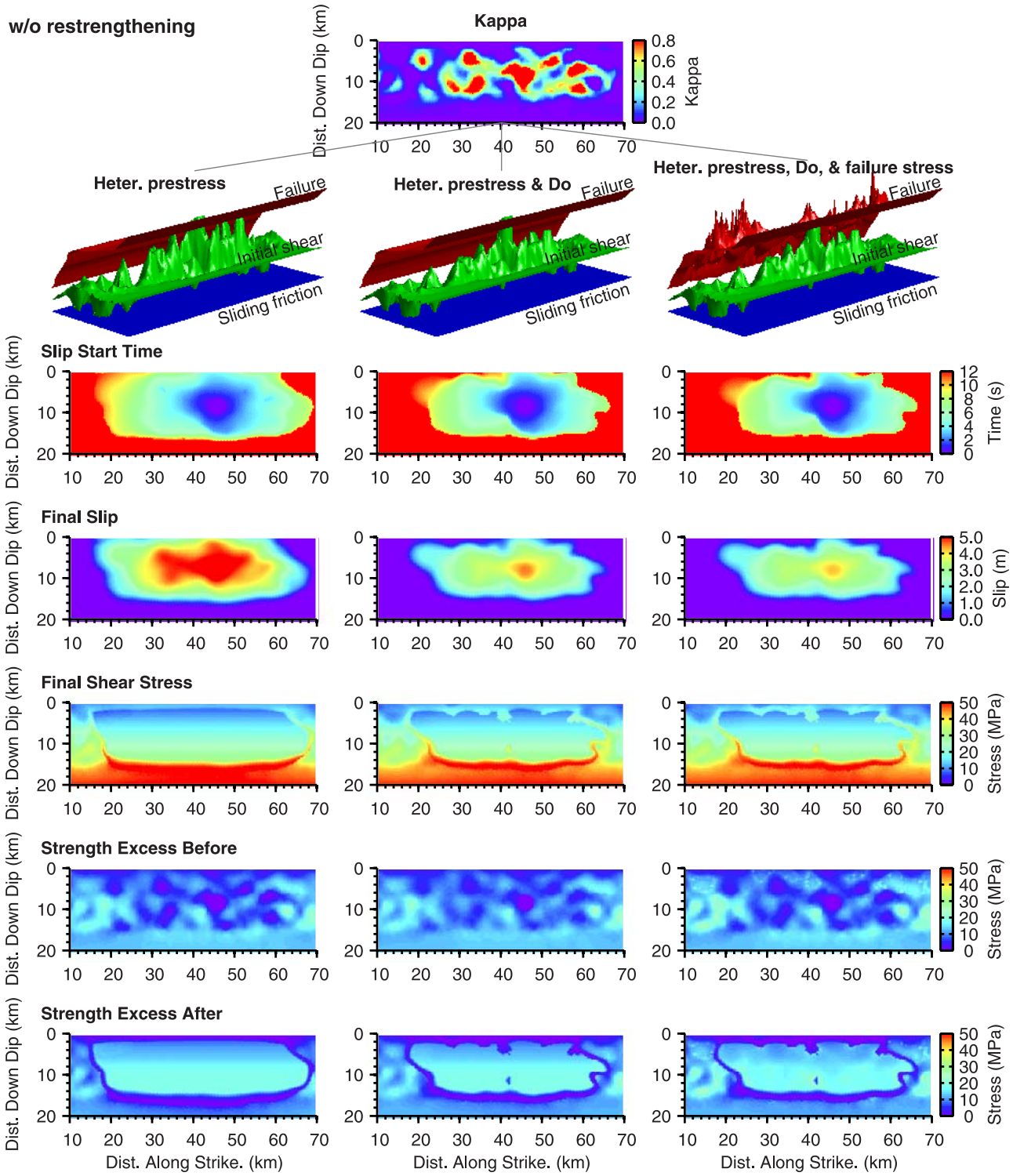

Figure 4. Comparison of initial conditions and rupture characteristics for three illustrative scenarios for slip-weakening friction without restrengthening. All scenarios use the same initial distribution of κ (top middle). The spatial variation in κ is associated with either variations in dynamic stress drop via the prestress ($\alpha_{dyn} = 1$; left), variations in dynamic stress drop via the prestress accompanied by variations in breakdown work via D_o ($\alpha_{dyn} = 0.75$, $\alpha_{fail} = 0$; middle), or variations in dynamic stress drop via the prestress accompanied by variations in breakdown work via both D_o and failure stress ($\alpha_{dyn} = 0.75$, $\alpha_{fail} = 0.25$; right).

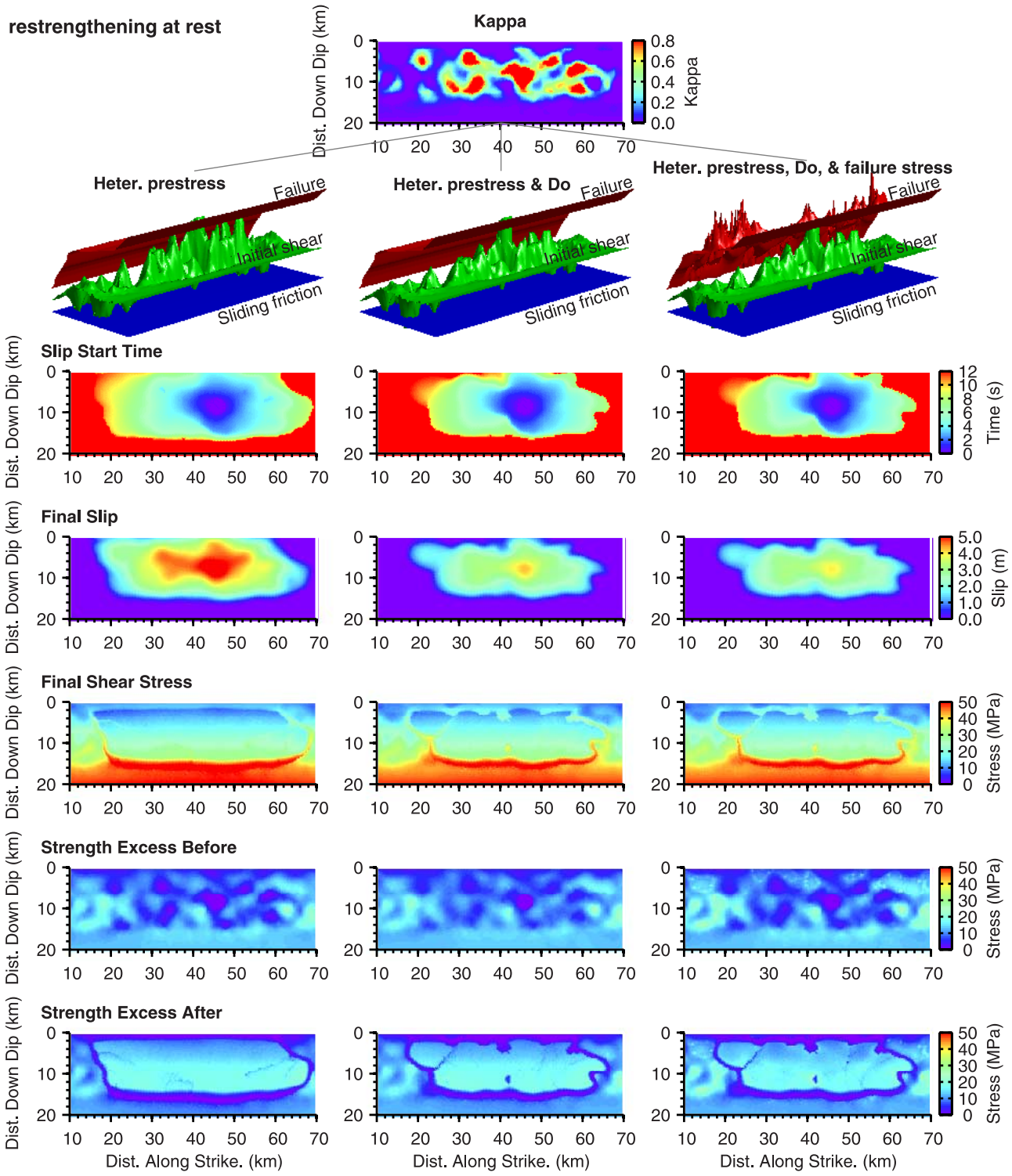

Figure 5. Comparison of initial conditions and rupture characteristics for three illustrative scenarios for slip-weakening friction with restrengthening at rest. All scenarios use the same initial distribution of κ (top middle). The spatial variation in κ is associated with either variations in dynamic stress drop via the prestress ($\alpha_{dyn} = 1$; left), variations in dynamic stress drop via the prestress accompanied by variations in breakdown work via D_o ($\alpha_{dyn} = 0.75$, $\alpha_{fail} = 0$; middle), or variations in dynamic stress drop via the prestress accompanied by variations in breakdown work via both D_o and failure stress ($\alpha_{dyn} = 0.75$, $\alpha_{fail} = 0.25$; right).

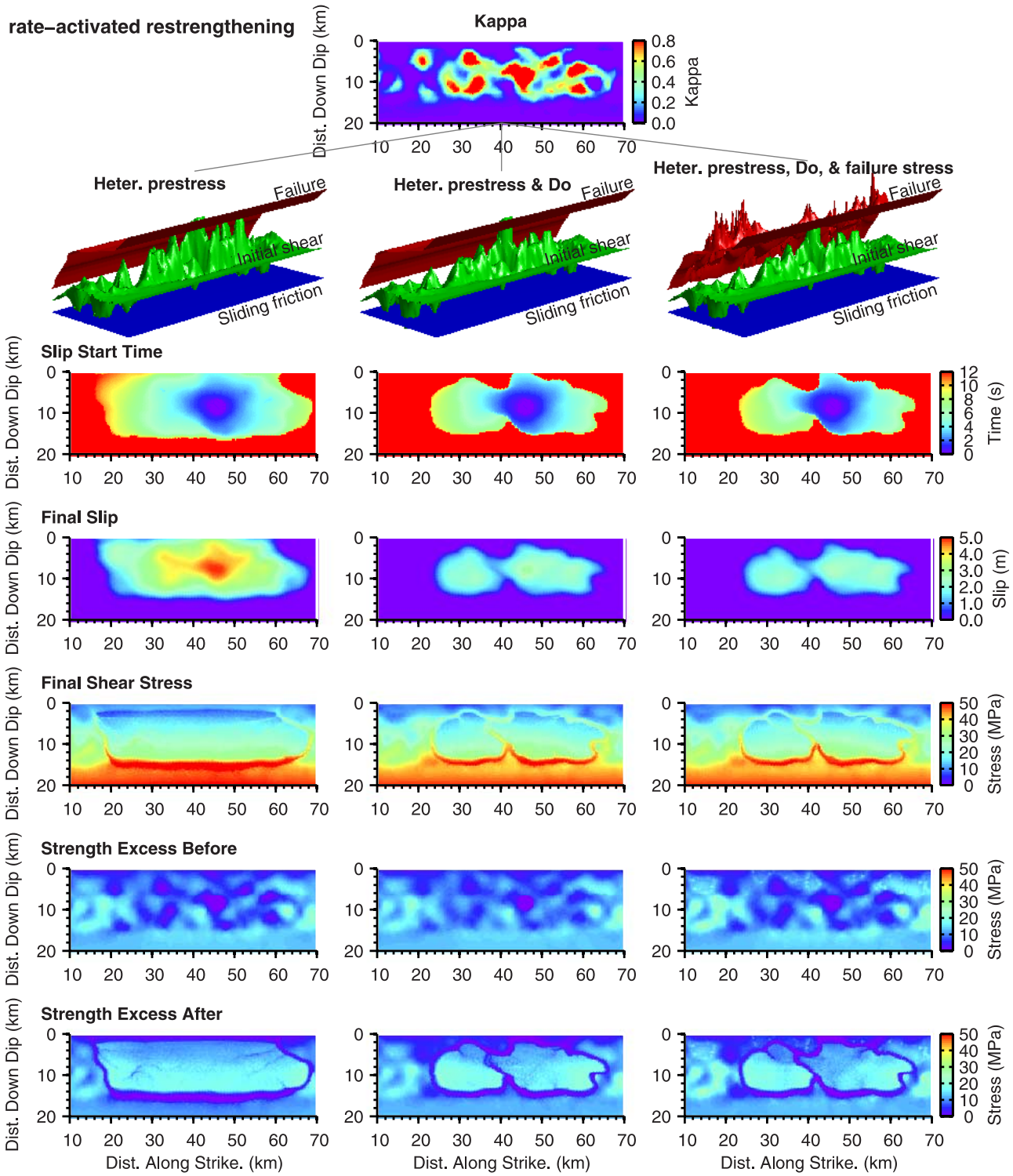

Figure 6. Comparison of initial conditions and rupture characteristics for three illustrative scenarios for slip-weakening friction with rate-activated restrengthening. All scenarios use the same initial distribution of κ (top middle). The spatial variation in κ is associated with either variations in dynamic stress drop via the prestress ($\alpha_{dyn} = 1$; left), variations in dynamic stress drop via the prestress accompanied by variations in breakdown work via D_o ($\alpha_{dyn} = 0.75$, $\alpha_{fail} = 0$; middle), or variations in dynamic stress drop via the prestress accompanied by variations in breakdown work via both D_o and failure stress ($\alpha_{dyn} = 0.75$, $\alpha_{fail} = 0.25$; right).

Table 5. Parameters and Rupture Characteristics for Each Scenario[a]

α_{dyn}	α_{fail}	Average Slip (m)	M_w	SD in Strength Excess,[b] $\times 10^{-4}$ Before	SD in Strength Excess,[b] $\times 10^{-4}$ After	Remarks
			Friction Model noR			
1.00	–	2.81	7.19	1.2	0.2	Inconsistent
0.75	0.00	1.99	7.04	1.0	0.2	Inconsistent
0.75	0.25	1.91	7.02	1.0	0.6	Marginally self-consistent
0.75	0.50	1.86	7.01	1.1	0.7	Marginally self-consistent
0.50	0.00	1.61	6.93	0.7	0.2	Inconsistent
0.50	0.25	1.51	6.89	1.0	0.7	Marginally self-consistent
0.50	0.50	1.44	6.86	1.2	0.8	Marginally self-consistent
0.25	0.00	1.34	6.85	0.5	0.2	Inconsistent
0.25	0.25	1.13	6.64	–	–	Small event (discarded)
0.25	0.50	0.63	6.23	–	–	Small event (discarded)
			Friction Model restR			
1.00	–	2.62	7.16	1.2	0.4	Inconsistent
0.75	0.00	1.81	7.01	0.9	0.5	Inconsistent
0.75	0.25	1.77	7.00	1.0	0.6	Marginally self-consistent
0.75	0.50	1.72	6.98	1.1	0.7	Marginally self-consistent
0.50	0.00	1.31	6.84	0.7	0.6	Self-consistent
0.50	0.25	1.22	6.66	–	–	Small event (discarded)
0.50	0.50	1.15	6.63	–	–	Small event (discarded)
0.25	0.00	1.04	6.59	–	–	Small event (discarded)
0.25	0.25	0.93	6.54	–	–	Small event (discarded)
0.25	0.50	0.60	6.20	–	–	Small event (discarded)
			Friction Model rateR			
1.00	–	2.35	7.12	1.2	0.6	Inconsistent
0.75	0.00	1.30	6.84	0.9	0.8	Self-consistent
0.75	0.25	1.29	6.83	1.0	0.7	Marginally self-consistent
0.75	0.50	1.23	6.68	–	–	Small event (discarded)
0.50	0.00	0.99	6.58	–	–	Small event (discarded)
0.50	0.25	0.94	6.56	–	–	Small event (discarded)
0.50	0.50	0.71	6.29	–	–	Small event (discarded)
0.25	0.00	0.71	6.25	–	–	Small event (discarded)
0.25	0.25	0.66	6.21	–	–	Small event (discarded)
0.25	0.50	0.52	6.10	–	–	Small event (discarded)

[a]The friction models noR, restR, and rateR refer to slip-weakening without restrengthening, slip-weakening with restrengthening at rest, and slip-weakening with rate-activated restrengthening, respectively.
[b]The values for the standard deviation in strength excess have been normalized by the shear modulus.

the nominal background stress. On the other hand, in real earthquakes the sliding friction likely does vary spatially and its absolute level and spatial variability become important in controlling slip and stress heterogeneity as inelastic deformation, heating, and other processes occur.

[27] The two trade-off parameters, α_{dyn} and α_{fail}, permit selecting from a continuous spectrum of initial conditions and fault constitutive parameters that match the selected spatial variation in κ. We consider four values for α_{dyn} and three values for α_{fail} covering a considerable range of the parameter space; Table 5 gives the values of the trade-off parameters for the 10 cases in this study. We consider these 10 cases for each of the three levels of shear restrengthening, yielding a total of 30 scenarios.

3. Results

[28] In each scenario the ruptures nucleate at a depth of 8.3 km at a location 43.4 km along strike from the left ($-y$) edge of the fault as a result of raising the shear stress to 2% above the failure stress over a circular region with a 2 km radius. This region is centered on the location where κ is at a maximum. Table 5 summarizes the basic characteristics of fault rupture in each of the 30 scenarios, while Figures 4–6 illustrate examples of the rupture behavior and conditions before and after rupture for the three levels of shear restrengthening. We succeed in producing 16 ruptures with similar rupture behavior: bilateral rupture with moment magnitudes in the range of 6.8 to 7.2 and similar spatial-temporal evolutions of slip.

[29] Figure 7 shows rupture propagation via snapshots of the slip rate 6.0 s after the ruptures begin, and Figure 8 demonstrates that the velocity time histories from these scenarios are quite similar, and in some cases nearly identical. It also shows how delayed rupture to the left ($-y$ direction) in a few of the scenarios affects the ground motions, indicating that such deviations in rupture behavior could be identified in a kinematic source inversion. The scenarios labeled "discarded" in Table 5 produce ruptures with significantly different behavior suggesting that other factors besides the value of κ influence the extent of rupture. For example, the ratio of the failure stress relative to the dynamic stress drop and the initial stress, as parameterized by the relative strength, $S = (\sigma_{fail} - \sigma_0)/(\sigma_0 - \sigma_{sliding})$ [*Andrews*, 1976a], is another nondimensional parameter that influences the ability of ruptures to propagate, particularly in discrete models that blunt the sharpness of the stress peak at the leading edge of the rupture.

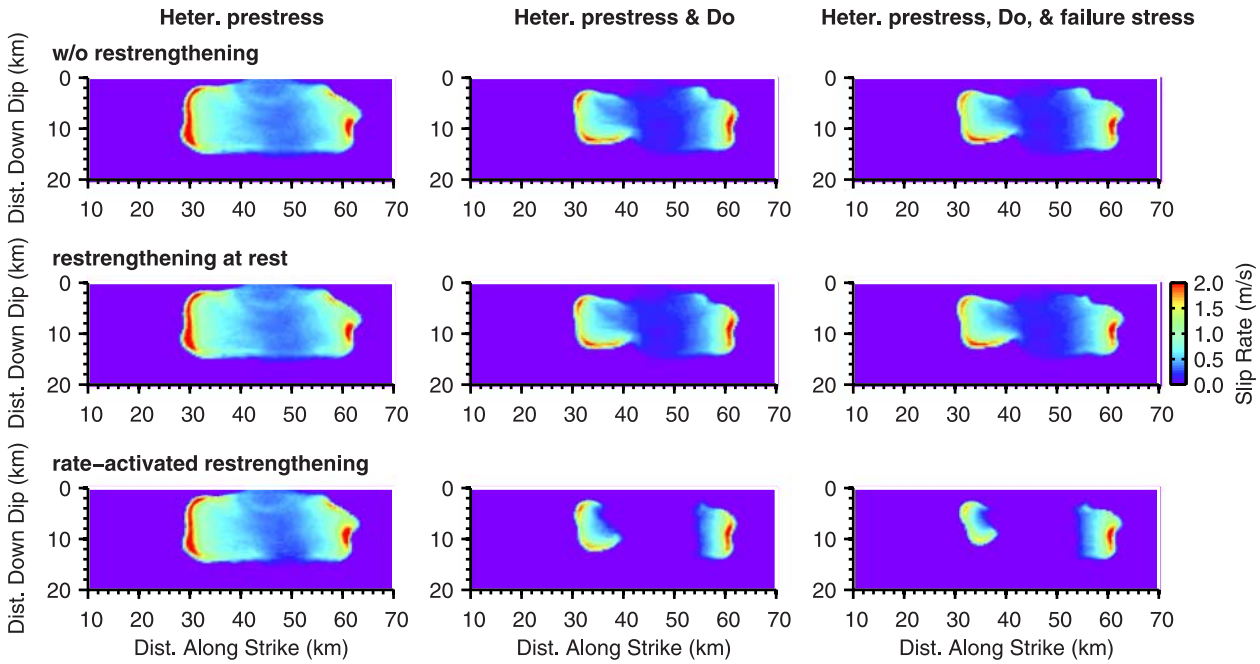

Figure 7. Snapshots of slip rate 6.0 s after rupture initiation for each of the nine scenarios in Figures 4–6, left to right corresponding to the same three different realizations of initial conditions and parameters shown in Figures 4–6 and the top to bottom corresponding to the three levels of restrengthening. Whereas the leading edges of the ruptures are very similar, the widths of the slip pulses differ significantly.

[30] Rupture propagation beginning at the hypocenter and proceeding to the left ($-y$ direction) is more difficult than that to the right ($+y$ direction) due to a large local minimum in κ just to the left of the hypocenter. As more of the spatial variation in κ is mapped into spatial variations in breakdown work and failure stress, small regions with locally large values of strength excess prove to be significant barriers for propagation in the discrete models. κ is inversely proportional to the breakdown work (and therefore the failure stress) but proportional to the square of the difference between initial shear stress and sliding friction. This means that variations in the dynamic stress drop (initial shear stress) result in relatively larger variations in κ than do variations in failure stress. Likewise, variations in κ arise from smaller variations in the dynamic stress drop (initial shear stress) compared with the failure stress (compare the red surfaces in Figures 4 (middle), 5 (middle), and 6 (middle)). As a result, mapping a significant portion of the spatial variation in κ into the failure stress ($\alpha_{dyn} \leq 0.5$) leads to dramatic variations in the failure stress preventing the ruptures from expanding beyond the nucleation region. This is why scenarios with $\alpha_{dyn} \leq 0.5$ produce earthquakes (in all but a couple cases) with average slips and moment magnitudes that are smaller than the target values. Additionally, the presence of shear restrengthening, which increases the friction as the slip rate becomes low or when sliding stops, tends to extinguish the rupture if it encounters any sort of barrier (locally small κ). This explains why the events tend to become smaller as more restrengthening is added to the fault constitutive model; rapid restrengthening promotes slip heterogeneity, which also increases the possibility of rupture termination [*Liu-Zeng et al.*, 2005].

[31] The presence of restrengthening permits the dynamic stress drop to be significantly larger than the static stress drop, but the difference between the dynamic and static stress drop is very small over most of the rupture area. This indicates that just a small rise in the dynamic sliding friction during slip can have a significant affect on the healing phases (i.e., pulse width) and whether or not the rupture propagates. However, for the pulse widths permitted with the spatial resolution of our models, it does not have a strong affect on the macroscopic rupture behavior and the conditions left behind by the rupture, aside from adding in a small amount of short-length-scale numerical noise. On the other hand, the spatial variations in the breakdown work (manifested in variations in the failure stress and slip-weakening parameter) create barriers that impede slip, resulting in final shear stress that differs significantly at many locations from the sliding stress. These barriers can lead to slight variations in rupture speed and slip rate as is evident in the more complex velocity time histories at sites A and B in Figure 8 for the cases with $\alpha_{dyn} \leq 0.75$, nevertheless the ground motions remain quite similar.

[32] We now focus our attention on the initial and final shear stress relative to the sliding friction and evaluate the consistency in the amount of heterogeneity. Our objective is to identify the sets of parameters conducive to generating "self-consistent" ruptures; as described earlier, we perceive self-consistent ruptures as those that begin with a heterogeneous shear stress field and leave behind a heterogeneous shear stress field. We quantify the degree of self-consistency by comparing the standard deviation in the normalized strength excess before and after rupture. At each point where slip occurs, we compute the strength excess (the

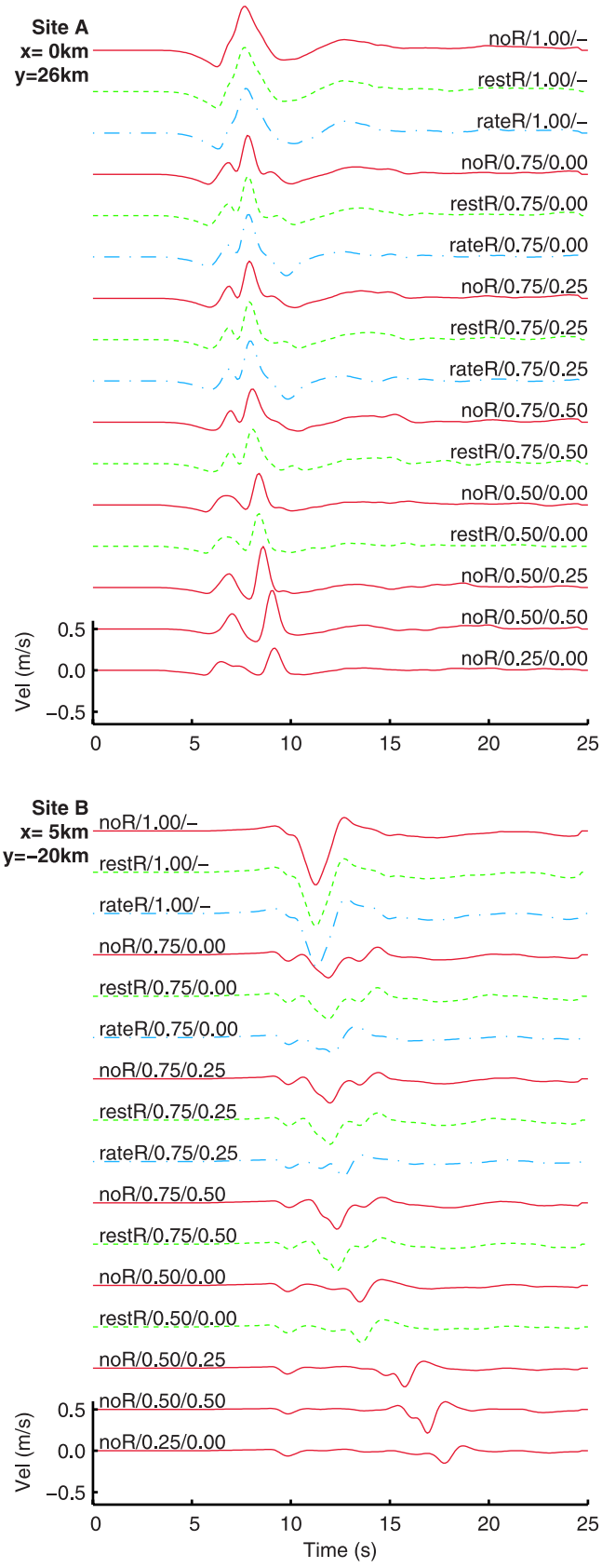

difference between the failure stress and the shear stress) and divide by the shear modulus to find the normalized strength excess. Before rupture, the distribution of normalized strength excess roughly matches a normal distribution, so it is straightforward to compute the standard deviation for each of the scenarios. The normalized strength excess after rupture is bimodal: a peak near zero corresponds to the edge of the rupture area, whereas a second peak corresponds to the area where the stress decreases as a result of the rupture. We focus on this second peak because the standard deviation with respect to this peak gives an indication of the heterogeneity in the stress field where rupture occurred. If the standard deviation decreases dramatically, then it indicates that the rupture removed heterogeneity in the shear stress field; we label these cases "inconsistent". On the other hand, if the standard deviation is about the same before and after rupture, then it indicates that the rupture maintained heterogeneity in the shear stress field; we label these cases "self-consistent". We label intermediate cases "marginally self-consistent."

[33] Figures 4–6 show the strength excess before and after rupture for nine of the scenarios, and Figure 9 displays the histograms of normalized strength excess over the rupture area for each of these scenarios. Table 5 lists the normalized strength excess of the rupture area for all 16 of the ruptures near the target size. The standard deviation of the normalized strength excess differs slightly from one scenario to another because the rupture areas differ. Figures 4 (left), 5 (left, 6 (left), and 9 (left) illustrate cases in which the initial shear stress is heterogeneous but the final shear stress field is homogeneous over the area where rupture occurred. As a result, the standard deviation in the normalized strength excess after rupture is very small, and we classify these three simulations as "inconsistent." Figures 4 (middle and right), 5 (middle and right), 6 (middle and right), and 9 (middle and right) demonstrate that as we distribute more of the spatial variation in κ into the breakdown work, the standard deviations in the normalized strength excess do not decrease as much, so we begin to retain heterogeneity in the stress field. Additionally, as we add restrengthening to the fault constitutive model and include rate-activated restrengthening, the ruptures tend to become more self-consistent. Furthermore, other realizations of spatially heterogeneous κ constructed in the same manner produce similar results. Including restrengthening also results in more discarded simulations for the cases in which we map at least 50% of the perturbations in κ into the breakdown work (giving rise to very large spatial variations in the failure stress and slip-weakening parameter) as discussed earlier.

Figure 8. Velocity time histories of the fault-perpendicular particle motion at two sites on the ground surface (see Figure 1) for the 16 scenarios with $M_w \geq 6.8$ ruptures (see Table 5). The labels indicate the friction model and the values for α_{dyn} and α_{fail}. The models with $\alpha_{dyn} \geq 0.75$ produce very similar rupture behavior and waveforms. The other scenarios have similar final slip distributions but take longer to break through the rupture barrier to the left ($-y$ direction), resulting in variations in waveform shape and timing.

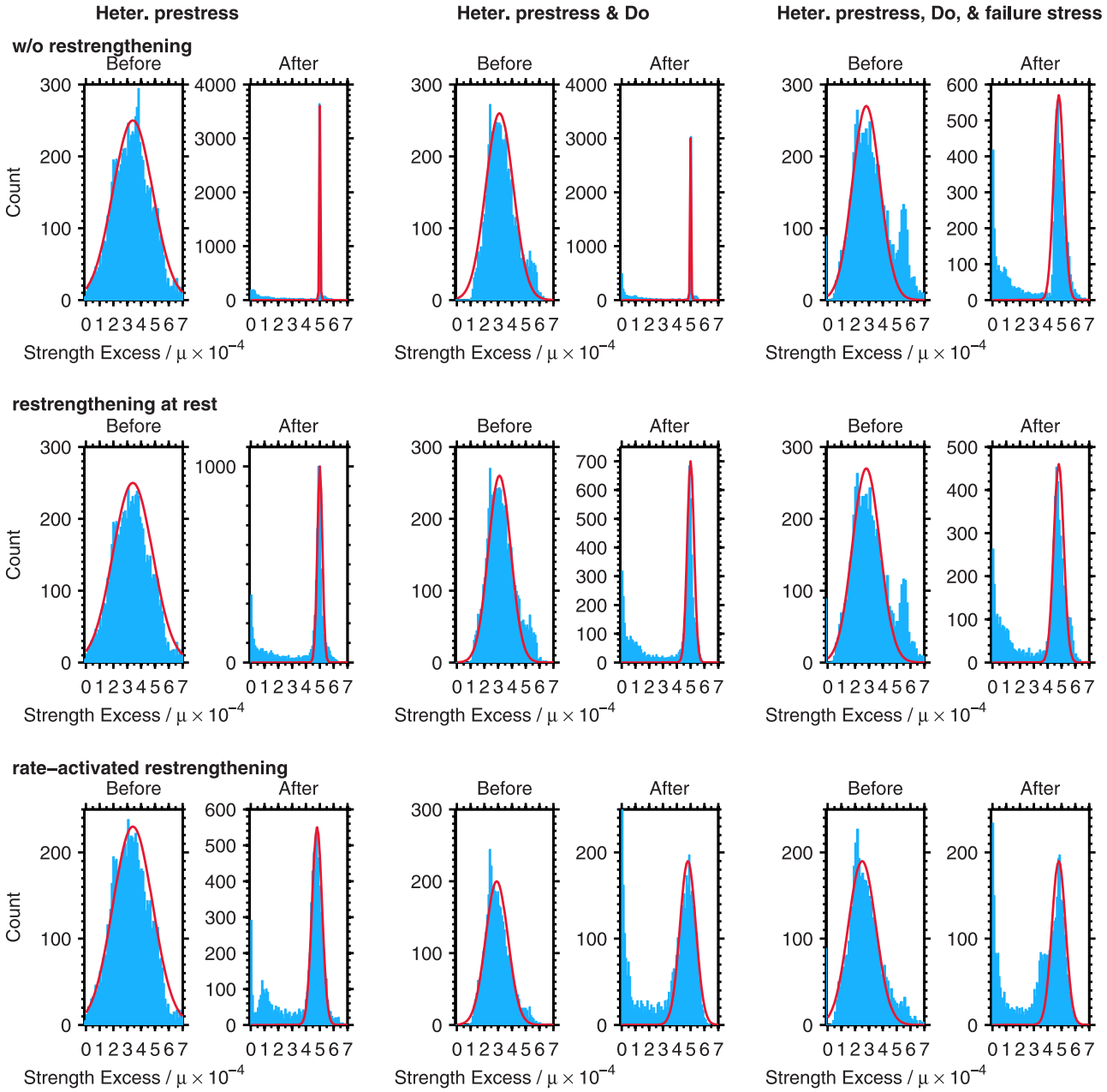

Figure 9. Histograms of normalized strength excess over the rupture area before and after rupture for each of the nine scenarios in Figures 4–6, with left to right corresponding to the same three different realizations of initial conditions and parameters shown in Figures 4–6 and top to bottom corresponding to the three levels of restrengthening. Including spatial heterogeneity in both the initial shear stress and breakdown work (especially in the failure stress) results in only slight decreases in the standard deviation, indicating the ruptures retain most of the heterogeneity in the stress field as desired.

[34] In all of the simulations slip is concentrated near the leading edge of the rupture front as shown in Figure 7. However, the total width of the slip pulses differs depending on the sources of heterogeneity (comparing columns) and the amount of restrengthening in the fault constitutive model (comparing rows). This means that the risetimes associated with the majority of the slip at a point are about the same, but the risetimes associated with the final slip values differ. Kinematic source inversions would not be able to detect these subtle differences, because the resulting ground motions are so similar. Incorporating spatial heterogeneity in both the dynamic stress drop (initial shear stress) and breakdown work trims the trailing edge of the slip pulse as does adding restrengthening to the fault constitutive model. One might expect the slip-weakening with rate-activated restrengthening model to consistently produce the narrowest slip pulses. Instead, the pulse width exhibits a dependence on both the spatial variation in the parameters and the presence of restrengthening in the fault constitutive model. Combining spatial variations in dynamic stress drop

and breakdown work aid the generation of healing fronts, contributing to narrow slip pulses.

4. Implications

[35] There are two important contexts in which to examine the results of these simulations. First, the simulations suggest some useful constraints on fault constitutive models for use in numerical simulations of earthquake ruptures that focus on reproducing realistic distributions of both slip and stress. Second, we consider how to extrapolate the numerical results, which span a limited range of scales, to the dynamics of natural earthquakes, which span a much broader range of scales.

4.1. Creating Realistic Numerical Simulations

[36] Our results imply that generating earthquake ruptures in numerical models consistent with the basic physics driving heterogeneous slip requires spatially heterogeneous fields for both the dynamic stress drop and breakdown work. Models with only heterogeneous dynamic stress drop can produce rupture behavior similar to those that include spatial heterogeneity in both, but the initial and final stress fields are not self-consistent. For example, the shear stresses in the scenarios with heterogeneous initial shear stresses and homogeneous breakdown work became homogeneous in the area where rupture occurred. Such models might be acceptable for use in studying ground motions, but they neglect complex spatial variations in the initial conditions and parameters that appear to play important roles in the physics of earthquake ruptures. As a result, we consider such models to be inconsistent with the conditions driving heterogeneous slip in earthquakes.

[37] In this study we focused on the spatial variability of the initial and final shear stresses relative to the sliding friction stress and considered spatial variations in dynamic stress drop arising from spatial variations in the initial shear stress alone. In the broader context of real earthquakes, we need to consider how such spatial variations in the dynamic stress drop might develop from spatial variations arising in either the shear stresses or the sliding friction. Seismologic observations support characterization of the stress field as heterogeneous both before and after rupture. The rapid onset of aftershocks, many of which appear to coincide with the main shock rupture surfaces [see, e.g., *Bakun et al.*, 2005; *Hauksson and Shearer*, 2005; *Langbein et al.*, 2005], suggests that the strength excess following an earthquake rupture is quite heterogeneous. Associating this heterogeneous strength excess with heterogeneity in the stress field would explain the presence of left-lateral aftershocks following the 1989 Loma Prieta earthquake, which had oblique right-lateral slip [*Oppenheimer*, 1990]. Stress tensor orientations inferred from focal mechanism inversions suggest that, in general, the stress field is spatially heterogeneous [*Hardebeck and Hauksson*, 2001a, 2001b]. Furthermore, *Smith* [2006, available at http://resolver.caltech.edu/CaltechETD:etd-05252006-191203] used a simple 3-D model of a heterogeneous stress field to explain the relationship among tectonic loading, stress perturbations due to earthquake rupture, and temporal variations in focal mechanisms. Stronger evidence for stress heterogeneity comes from measurements of crustal stress from the Cajon Pass and KTB boreholes, which support characterization of the crustal stress field as a fractal distribution [*Marsan and Bean*, 2003].

[38] We do not have similar evidence for spatial heterogeneity in the sliding friction or breakdown work, because in situ measurements of spatial variations of these quantities are, unfortunately, not currently practical. *Madariaga* [1983] suggested that heterogeneous breakdown work could explain high-frequency radiation. While the analysis was limited to a semi-infinite crack, we expect heterogeneous breakdown work has a similar affect on narrow slip pulses. Several studies [*Guatteri et al.*, 2003; *Ide*, 2003; *Tinti et al.*, 2005] have made indirect estimates of the spatial variations in breakdown work using the slip-weakening model and seismologic data. Additional indirect evidence for the possible existence of spatial variations in sliding friction and breakdown work comes from studies of complex fault geometry, such as irregular nonplanar surfaces, bends, and junctions [*Segall and Pollard*, 1980; *Andrews*, 1989; *Saucier et al.*, 1992; *Harris and Day*, 1993; *Bouchon*, 1997; *Nielsen and Knopoff*, 1998]. It is relatively straightforward to include nonplanar fault geometry at length scales much larger than the discretization size in numerical simulations, but it is not clear how to implement geometrically complex fault surfaces at small scales or the physics associated with slip on such surfaces [*Harris*, 2004]. Recent attempts to develop equivalent planar representations of kinks or bends with fault surfaces have had marginal success [*Kase and Day*, 2006; *Madariaga et al.*, 2006].

[39] In our simulations we find that restrengthening may not be an essential ingredient for producing self-consistent behavior, but it does expand the range of conditions under which ruptures exhibit self-consistent behavior. The most important ingredient for developing self-consistent ruptures appears to be narrow slip pulses. Including spatial heterogeneity in the breakdown work in addition to the dynamic stress drop produces narrow slip pulses, independent of the presence or absence of restrengthening. This is not unexpected given that several previous studies have shown that heterogeneous stress fields and rate-independent friction are compatible with the pulse-like behavior imaged in kinematic source inversions [*Das and Aki*, 1977; *Papageorgiou and Aki*, 1983; *Beroza and Mikumo*, 1996; *Ide and Takeo*, 1997; *Day et al.*, 1998; *Fukuyama and Madariaga*, 1998; *Oglesby and Day*, 2002].

[40] In this study we use a rather simple test for gauging whether the ruptures are self-consistent. A more rigorous test could involve modeling multiple earthquake cycles that include strain accumulation, strain release through the propagation of ruptures, and postseismic relaxation. In such simulations one can examine long-term trends and quantify any significant changes in the spectral character of the distributions of slip over time. This approach is attractive because several studies [e.g., *Somerville et al.*, 1999; *Mai and Beroza*, 2002; *Lavallée and Archuleta*, 2003; *Liu-Zeng et al.*, 2005] have focused on characterizing the spectral character of slip distributions. Additionally, aftershocks, events on adjacent portions of the fault, and nonuniform loading, which might all influence the evolution of the stress field, could also be included.

[41] Some work with multicycle earthquake simulations has been done for simplistic 2-D [e.g., *Shaw*, 1997; *Lapusta*

et al., 2000], and 3-D problems [*Liu and Lapusta*, 2005], but they do not address the question of slip heterogeneity. These simulations can be computationally intensive, because they must include nucleation of ruptures as fault loading increases (e.g., acceleration of slip within a confined zone as a result of loading and rate and state friction [*Tse and Rice*, 1986; *Okubo*, 1989; *Dieterich*, 1992]). This means that we must have sufficient spatial and temporal resolution to capture the slow buildup of strain and its sudden release in propagating ruptures (so that the modeling incorporates 3-D effects known to be important in studying rupture propagation [e.g., *Harris*, 2004, and references therein] and viscoelastic deformation [e.g., *Yoshioka and Suzuki*, 1999; *Freed and Lin*, 2001; *Wang et al.*, 2001; *Hearn et al.*, 2002]). As these multicycle models become more comprehensive and approach the complexity necessary to provide additional constraints on fault constitutive models, the number of small events generated on the fault system will tend to increase in accordance with the Gutenberg-Richter frequency-magnitude relationship. This could easily lead to time consuming calculations with a large fraction of the time spent resolving slip in small events while waiting for the large events (which are of primary interest) to occur. However, these small events could also contribute to the spatial heterogeneity of the stress field and slip heterogeneity in subsequent large events.

4.2. Conjectures on Earthquake Rupture Dynamics

[42] Numerical simulations that span a limited range of scales, such as those in this study, make direct comparisons to earthquake ruptures difficult. However, they do provide a useful tool for examining basic questions about the physics of earthquake rupture dynamics and can guide our inferences about rupture dynamics across a broader range of scales.

[43] An important feature in our suite of simulations is the presence of narrow slip pulses when we combine heterogeneous breakdown work (manifested in variations in the failure stress and slip-weakening parameter) with a heterogeneous dynamic stress drop. *Heaton* [1990] postulated that slip pulses arise from rate dependent restrengthening. In our simple fault constitutive model, restrengthening certainly appears to help confine slip pulses, but it does not lead to narrow, confined slip pulses by itself as illustrated in Figure 7. Formulations that more directly integrate restrengthening into the evolution of friction stress so that there is stronger feedback between slip, slip rate, and restrengthening might produce narrow slip pulses under a broader range of conditions (e.g., with a homogeneous spatial distribution of breakdown work). Additionally, dynamic processes that may produce slip pulses, such as the formation of silica gel [*Di Toro et al.*, 2004] or flash heating, tend to create large changes in friction; coefficients of friction in rotary shear experiments often drop quickly from about 0.6 to near 0.2 [*Di Toro et al.*, 2004]. These rapid friction stress changes would give rise to breakdown zones perhaps only a few meters in size; resolving such small-scale features with current numerical techniques would require discretization sizes a meter or smaller in size. Since the number of floating point operations increases by a factor of 16 for each power of two decrease in discretization size, we will need more than larger, faster computers to resolve features that are a few meters in size.

[44] If we could remove the length-scale limitations in our numerical models, what features would they have? Guided by observations of narrow slip pulses and rate restrengthening with our results from generating self-consistent ruptures, we make the following conjecture: in addition to fractal distributions of slip, narrow slip pulses driven by strongly rate-dependent friction propagating through a highly heterogeneous fractal stress field can produce (1) rapid changes in friction from high static values to low dynamic values and (2) radiated energy that is much larger than the breakdown work. In other words, we hypothesize that slip heterogeneity is controlled primarily by the complex interplay between the heterogeneous prestress and the inherent instability of a strong rate dependence in fault constitutive behavior. Heterogeneity in the stress field is maintained by the slip heterogeneity that occurs in each event. This hypothesis of earthquake rupture seems consistent with several entangling geophysical observations.

[45] Numerous studies have demonstrated that rate-dependent friction is compatible with a heterogeneous stress field and heterogeneous slip [e.g., *Cochard and Madariaga*, 1994, 1996; *Fukuyama and Madariaga*, 1998]. A strong rate dependence is also attractive because, as discussed earlier, it permits a rapid decrease in friction from high static values to low dynamic sliding values. This resolves the heat paradox and matches observations of low heat production on millimeter-wide primary slip surfaces [*Chester and Chester*, 1998]. Rapid restrengthening provides the ability to lock in heterogeneous stresses compatible with generating aftershocks with widely varying focal mechanisms, including those with left-lateral slip following the 1989 Loma Prieta earthquake, which had oblique right-lateral slip [*Oppenheimer*, 1990]. Fluctuations in rupture speed would arise not from spatial variations in breakdown work but from variations in the dynamic stress drop. Areas with negative dynamic stress drops would absorb energy and slow rupture propagation while areas with positive dynamic stress drops would release energy and accelerate rupture propagation much in the same way that relatively larger and smaller breakdown work do. This trade-off is evident in the expression for κ via the ratio $(\sigma_0 - \sigma_{sliding})^2/W_b$. This would permit ruptures to have relatively small, homogeneous breakdown work, comparable to rock mechanics' estimates of fracture energy from the Punchbowl fault of $7-50$ kJ/m^2, which are much lower than typical seismologic estimates of breakdown work of about 1 MJ/m^2 [*Chester et al.*, 2005].

[46] A possible counterargument to this conjecture may be the rise times inferred from near-field ground motion records. Our current best estimates of risetime in large earthquakes come from the near-source ground motion records for the 1999 M_w 7.6 Chi-Chi, Taiwan, earthquake and the 2002 M_w 7.9 Denali fault, Alaska, earthquake; yet, even these can be error prone due to the kilometer or more distances of stations from the fault rupture and near-surface effects associated with the surface rupture affecting the slip pulse. The TCU052 and TCU068 vertical velocity records from the Chi-Chi earthquake [*Boore*, 2001] suggest the risetime on the fault near each of the stations was about 5 s. These two records, however, may give a distorted estimate of the risetime because the records from the northern end of the Chi-Chi rupture have much more

long-period energy than empirical equations based on data from events in California [*Boore*, 2001]. Analysis of the Pump Station 10 (PS10) record in the Denali earthquake gives a risetime of 3 s [*Dunham and Archuleta*, 2004; *Ellsworth et al.*, 2004]. In this case, the presence of supershear rupture helps preserve the slip time function in the near-source ground motions, yielding a relatively clearer picture of the risetime [*Dunham and Archuleta*, 2004]. These two estimates of risetime are similar to those in our numerical models and would be longer than those we are proposing. However, *Kagawa et al.* [2004] found evidence suggesting that risetimes near the surface appear to be larger than those at depth, which could bias estimates of risetime based on near-source ground motions recorded at the surface to larger values.

[47] Near-source records for magnitude 6–8 events from deep boreholes should be less susceptible to near-surface effects and changes in rupture dynamics at shallow depths, but few such boreholes exist due to their high costs. While we wait for better data sets for magnitude 6–8 events, improved images of rupture propagation might be available from the San Andreas Observatory at Depth (SAFOD) in central California. SAFOD [*Hickman et al.*, 2004] intends to capture the ground motions from magnitude 2 events at a range of a few hundred meters at a depth of about 2 kilometers. While the slip will be small, these recordings should alleviate near-surface effects and could place tighter constraints on the minimum risetime (and slip pulse width) of larger events and provide evidence for how risetimes vary with earthquake size (assuming SAFOD succeeds in capturing high-resolution images of other events of various sizes).

[48] Because of Earth's complex structure, we expect future studies will show that spatial variations in the stress field along with relatively narrow slip pulses work together to produce heterogeneous slip in earthquakes and sustain a heterogeneous crustal stress field over time. A more thorough understanding of rupture dynamics will require characterizing the physical processes associated with these features, and in particular, how rapid spatial and temporal changes in friction resulting from dynamic processes contribute to the formation of narrow slip pulses and slip heterogeneity.

Appendix A: Mapping Heterogeneity in κ Into Parameters

[49] We want to map spatial variations in κ into spatial variations in the parameters on which it depends. Of course, the variations could all be independent, but if they are not then we would like to determine their relative contributions, which is what we want to do in this study.

[50] Let $f(x, y)$ be a function with some variation about its nominal value $f^* = f(x^*, y^*)$. Consider $f(x, y) = x + y$. We know that $\partial f = \partial x + \partial y$, so we expect the variation in $f(x, y)$ to be the sum of the variations in x and y. We can show that

$$x = x^* + \alpha(f(x,y) - f^*), \tag{A1}$$

$$y = y^* + (1 - \alpha)(f(x,y) - f^*), \tag{A2}$$

where

$$\alpha \in [0, 1] \tag{A3}$$

satisfies $f(x, y) = x + y$ and $\partial f = \partial x + \partial y$.

[51] If $f(x, y) = xy$, we can use the fact that $\log f = \log x + \log y$ to show that

$$\log\left(\frac{x}{x^*}\right) = \alpha \log\left(\frac{f(x,y)}{f^*}\right), \tag{A4}$$

or

$$x = x^* \left(\frac{f(x,y)}{f}\right)^{\alpha}. \tag{A5}$$

[52] Starting with the ratio of κ to κ^*,

$$\frac{\kappa}{\kappa^*} = \frac{\left(\sigma_0 - \sigma_{sliding}\right)^2 L}{W_b \mu} \frac{W_b^* \mu}{\left(\sigma_0^* - \sigma_{sliding}^*\right)^2 L}, \tag{A6}$$

we define α_{dyn} to be the logarithmic fraction of the perturbation in κ associated with perturbations in the dynamic stress drop,

$$\alpha_{dyn} = 2 \log\left(\frac{\sigma_0 - \sigma_{sliding}}{\sigma_0^* - \sigma_{sliding}^*}\right) / \log\left(\frac{\kappa}{\kappa^*}\right). \tag{A7}$$

Rearranging and solving the for the dynamic stress drop and breakdown work gives

$$\frac{\sigma_0 - \sigma_{sliding}}{\mu} = \left(\frac{\sigma_0^* - \sigma_{sliding}^*}{\mu}\right)\left(\frac{\kappa}{\kappa^*}\right)^{\frac{\alpha_{dyn}}{2}}. \tag{A8}$$

[53] From equations (A6) and (A7), we also have

$$\alpha_{dyn} - 1 = \log\left(\frac{W_b}{W_b^*}\right) / \log\left(\frac{\kappa}{\kappa^*}\right), \tag{A9}$$

which relates the perturbation in κ to spatial variations in the breakdown work. The breakdown work as a function of the failure stress, sliding stress, and slip-weakening parameter is

$$W_b = \frac{1}{2}\left(\sigma_{fail} - \sigma_{sliding}\right) D_0. \tag{A10}$$

Following the same procedure we used earlier for κ, the perturbation in the breakdown work is

$$\log\left(\frac{W_b}{W_b^*}\right) = \log\left(\frac{\sigma_{fail} - \sigma_{sliding}}{\sigma_{fail}^* - \sigma_{sliding}^*}\right) + \log\left(\frac{D_0}{D_0^*}\right), \tag{A11}$$

and we define α_{fail} to be the logarithmic fraction of the perturbation in the breakdown work associated with perturbations in the failure stress,

$$\alpha_{fail} = \log\left(\frac{\sigma_{fail} - \sigma_{sliding}}{\sigma_{fail}^* - \sigma_{sliding}^*}\right) / \log\left(\frac{W_b}{W_b^*}\right). \tag{A12}$$

Solving for the failure stress relative to the sliding stress and using equation (A9) yields

$$\frac{\sigma_{fail} - \sigma_{sliding}}{\mu} = \left(\frac{\sigma^*_{fail} - \sigma^*_{sliding}}{\mu}\right)\left(\frac{\kappa}{\kappa^*}\right)^{\alpha_{fail}\left(\alpha_{dyn}-1\right)}. \quad \text{(A13)}$$

From equations (A11) and (A12) we also have

$$1 - \alpha_{fail} = \log\left(\frac{D_0}{D_0^*}\right) / \log\left(\frac{W_b}{W_b^*}\right), \quad \text{(A14)}$$

which leads to

$$D_0 = D_0^*\left(\frac{\kappa}{\kappa^*}\right)^{\left(1-\alpha_{fail}\right)\left(\alpha_{dyn}-1\right)}. \quad \text{(A15)}$$

[54] **Acknowledgments.** We thank Ruth Harris, Paul Spudich, and an anonymous reviewer for comments which led to significant improvements in the manuscript.

References

Aagaard, B. T., T. H. Heaton, and J. F. Hall (2001), Dynamic earthquake ruptures in the presence of lithostatic normal stresses: Implications for friction models and heat production, *Bull. Seismol. Soc. Am.*, *91*(6), 1765–1796.

Aagaard, B. T., G. Anderson, and K. W. Hudnut (2004), Dynamic rupture modeling of the transition from thrust to strike-slip motion in the 2002 Denali Fault, Alaska, earthquake, *Bull. Seismol. Soc. Am.*, *94*(6B), S190–S201, doi:10.1785/0120040614.

Anderson, G., B. Aagaard, and K. Hudnut (2003), Fault interactions and large complex earthquakes in the Los Angeles area, *Science*, *302*(5652), 1946–1949.

Andrews, D. J. (1976a), Rupture propagation with finite stress in antiplane strain, *J. Geophys. Res.*, *81*(20), 3575–3582.

Andrews, D. J. (1976b), Rupture velocity of plane strain shear cracks, *J. Geophys. Res.*, *81*(32), 5679–5687.

Andrews, D. J. (1989), Mechanics of fault junctions, *J. Geophys. Res.*, *94*(B7), 9389–9397, doi:10.1029/89JB00774.

Andrews, D. J. (2004), Rupture models with dynamically determined breakdown displacement, *Bull. Seismol. Soc. Am.*, *94*(3), 769–775, doi:10.1785/0120030142.

Andrews, D. J., and R. A. Harris (2005), The wrinkle-like slip pulse is not important in earthquake dynamics, *Geophys. Res. Lett.*, *32*, L23303, doi:10.1029/2005GL023996.

Bakun, W. H., et al. (2005), Implications for prediction and hazard assessment from the 2004 Parkfield earthquake, *Nature*, *437*, 969–974, doi:10.1038/nature04067.

Beroza, G. C., and T. Mikumo (1996), Short slip duration in dynamic rupture in the presence of heterogeneous fault properties, *J. Geophys. Res.*, *101*(B10), 22,449–22,460.

Boore, D. M. (2001), Comparisons of ground motions from the 1999 Chi-Chi earthquake with empirical predictions largely based on data from California, *Bull. Seismol. Soc. Am.*, *91*(5), 1212–1217.

Bouchon, M. (1997), The state of stress on some faults of the San Andreas system as inferred from near-field strong motion data, *J. Geophys. Res.*, *102*(B6), 11,731–11,744.

Brodsky, E. E., and H. Kanamori (2001), Elastohydrodynamic lubrication of faults, *J. Geophys. Res.*, *106*(B8), 16,357–16,374.

Brune, J. N., S. Brown, and P. A. Johnson (1993), Rupture mechanism and interface separation in foam rubber models of earthquakes—A possible solution to the heat-flow paradox and the paradox of large overthrusts, *Tectonophysics*, *218*(1–3), 59–67.

Chester, F. M., and J. S. Chester (1998), Ultracataclasite structure and friction processes of the Punchbowl fault, San Andreas system, California, *Tectonophysics*, *295*(1–2), 199–221.

Chester, J., F. Chester, and A. K. Kronenberg (2005), Fracture surface energy of the Punchbowl fault, San Andreas system, *Nature*, *437*, 133–136, doi:10.1038/nature03942.

Cochard, A., and R. Madariaga (1994), Earthquake source mechanics and fracture mechanics: Theory and observation, *Pure Appl. Geophys.*, *142*(3–4), 419–445, doi:10.1007/BF00876049.

Cochard, A., and R. Madariaga (1996), Complexity of seismicity due to highly rate-dependent friction, *J. Geophys. Res.*, *101*(B11), 25,321–25,336.

Das, S., and K. Aki (1977), Fault plane with barriers: A versatile earthquake model, *J. Geophys. Res.*, *82*(36), 5658–5670.

Day, S. M. (1982), Three-dimensional simulation of spontaneous rupture: The effect of nonuniform prestress, *Bull. Seismol. Soc. Am.*, *72*(6), 1881–1902.

Day, S. M., G. Yu, and D. J. Wald (1998), Dynamic stress change during earthquake rupture, *Bull. Seismol. Soc. Am.*, *88*(2), 512–522.

Dieterich, J. H. (1979), Modeling of rock friction: 1. Experimental results and constitutive equations, *J. Geophys. Res.*, *84*(B5), 2161–2168.

Dieterich, J. H. (1992), Earthquake nucleation on faults with rate-dependent and state-dependent strength, *Tectonophysics*, *211*(1–4), 115–134.

Di Toro, G., D. L. Goldsby, and T. E. Tullis (2004), Friction falls towards zero in quartz rock as slip velocity approaches seismic rates, *Nature*, *427*, 436–439, doi:10.1038/nature02249.

Dunham, E. M., and R. J. Archuleta (2004), Evidence for a supershear transient during the 2002 Denali earthquake, *Bull. Seismol. Soc. Am.*, *68*(6B), S256–S268, doi:10.1785/0120040616.

Ellsworth, W. L., M. Celebi, J. R. Evans, E. G. Jensen, M. C. Metz, D. J. Nyman, J. W. Roddick, P. Spudich, and C. D. Stephens (2004), Near-field ground motions of the M 7.9 November 3, 2002, Denali Fault, Alaska, earthquake recorded at pump station 10, *Earthquake Spectra*, *20*(3), 597–615.

Freed, A. M., and J. Lin (2001), Delayed triggering of the 1999 Hector Mine earthquake by viscoelastic stress transfer, *Nature*, *411*, 180–183.

Fukuyama, E., and R. Madariaga (1998), Rupture dynamics of a planar fault in a 3-D elastic medium: Rate- and slip- weakening friction, *Bull. Seismol. Soc. Am.*, *88*(1), 1–17.

Guatteri, M., and P. Spudich (1998), Coseismic temporal changes of slip direction: The effect of absolute stress on dynamic rupture, *Bull. Seismol. Soc. Am.*, *88*(3), 777–789.

Guatteri, M., and P. Spudich (2000), What can strong-motion data tell us about slip-weakening fault-friction laws?, *Bull. Seismol. Soc. Am.*, *90*(1), 98–116.

Guatteri, M. P., M. Mai, G. C. Beroza, and J. L. Boatwright (2003), Strong ground-motion prediction from stochastic-dynamic source models, *Bull. Seismol. Soc. Am.*, *93*(1), 301–313.

Hardebeck, J. L., and E. Hauksson (2001a), Crustal stress field in southern California and its implications for fault mechanics, *J. Geophys. Res.*, *106*(B10), 21,859–21,882.

Hardebeck, J. L., and E. Hauksson (2001b), Stress orientations obtained from earthquake focal mechanisms: What are appropriate uncertainty estimates?, *Bull. Seismol. Soc. Am.*, *91*(2), 250–262, doi:10.1785/0120000032.

Harris, R. A. (2004), Numerical simulations of large earthquakes: Dynamic rupture propagation on heterogeneous faults, *Pure Appl. Geophys.*, *161*(11–12), 2171–2181, doi:10.1007/s00024-004-2556-8.

Harris, R. A., and R. J. Archuleta (2004), Seismology: Earthquake rupture dynamics: Comparing the numerical simulation methods, *Eos Trans. AGU*, *85*(34), 321.

Harris, R. A., and S. M. Day (1993), Dynamics of fault interaction: Parallel strike-slip faults, *J. Geophys. Res.*, *98*(B3), 4461–4472.

Hauksson, E., and P. Shearer (2005), Southern California hypocenter relocation with waveform cross-correlation, part 1: Results using the double-difference method, *Bull. Seismol. Soc. Am.*, *95*(3), 896–903, doi:10.1785/0120040167.

Hearn, E. H., R. Burgmann, and R. E. Reilinger (2002), Dynamics of Izmit earthquake postseismic deformation and loading of the Duzce earthquake hypocenter, *Bull. Seismol. Soc. Am.*, *92*(1), 172–193.

Heaton, T. H. (1990), Evidence for and implications of self-healing pulses of slip in earthquake rupture, *Phys. Earth Planet. Inter.*, *64*(1), 1–20.

Hickman, S., M. Zoback, and W. Ellsworth (2004), Introduction to special section: Preparing for the San Andreas Fault Observatory at depth, *Geophys. Res. Lett.*, *31*, L12S01, doi:10.1029/2004GL020688.

Ida, Y. (1972), Cohesive force across the tip of a longitudinal-shear crack and Griffith's specific surface energy, *J. Geophys. Res.*, *77*(20), 3796–3805.

Ide, A., and M. Takeo (1997), Determination of constitutive relations of fault slip based on seismic wave analysis, *J. Geophys. Res.*, *102*(B12), 27,379–27,391.

Ide, S. (2003), Fracture surface energy of natural earthquakes from the view of seismic observations, *Bull. Seismol. Soc. Am.*, *78*, 59–65.

Kagawa, T., K. Irikira, and P. G. Somerville (2004), Differences in ground motion and fault rupture process between the surface and buried rupture earthquakes, *Earth Planets Space*, *56*(1), 3–14.

Kase, Y., and S. M. Day (2006), Spontaneous rupture processes on a bending fault, *Geophys. Res. Lett.*, *33*, L10302, doi:10.1029/2006GL025870.

Langbein, J., et al. (2005), Preliminary report on the 28 September 2004, M 6.0 Parkfield, California earthquake, *Seismol. Res. Lett.*, *76*(1), 10–26.

Lapusta, N., J. R. Rice, Y. Ben-Zion, and G. T. Zheng (2000), Elastodynamic analysis for slow tectonic loading with spontaneous rupture episodes on faults with rate- and state-dependent friction, *J. Geophys. Res.*, *105*(B10), 23,765–23,789.

Lavallée, D., and R. J. Archuleta (2003), Stochastic modeling of slip spatial complexities for the 1979 Imperial Valley, California, earthquake, *Geophys. Res. Lett.*, *30*(5), 1245, doi:10.1029/2002GL015839.

Liu, Y., and N. Lapusta (2005), Three-dimensional simulations of spontaneous earthquake sequences, *Eos Trans. AGU*, *86*(52), Fall Meet. Suppl., Abstract S43A-1068.

Liu-Zeng, J., T. Heaton, and C. DiCaprio (2005), The effect of slip variability on earthquake slip-length scaling, *Geophys. J. Int.*, *162*(3), 841–849, doi:10.1111/j.1365-246X.2005.02679.x.

Madariaga, R. (1983), High frequency radiation from dynamic earthquake fault models, *Ann. Geophys.*, *1*, 17–23.

Madariaga, R., and A. Cochard (1994), Seismic source dynamics, heterogeneity and friction, *Ann. Geofis.*, *37*(6), 1349–1375.

Madariaga, R., and K. B. Olsen (2000), Criticality of rupture dynamics in 3-D, *Pure Appl. Geophys.*, *157*(11–12), 1981–2001.

Madariaga, R., J. P. Ampuero, and M. Adda-Bedia (2006), Seismic radiation from simple models of earthquakes, in *Earthquakes: Radiated Energy and the Physics of Faulting*, *Geophys. Monogr. Ser.*, vol. 170, edited by R. Abercrombie et al., pp. 223–236, AGU, Washington, D. C.

Magistrale, H., S. Day, R. W. Clayton, and R. Graves (2000), The SCEC southern California reference three-dimensional seismic velocity model version 2, *Bull. Seismol. Soc. Am.*, *90*(6), S65–S76.

Mai, P. M., and G. C. Beroza (2002), A spatial random field model to characterize complexity in earthquake slip, *J. Geophys. Res.*, *107*(B11), 2308, doi:10.1029/2001JB000588.

Marsan, D., and C. J. Bean (2003), Multifractal modeling and analyses of crustal heterogeneity, in *Heterogeneity in the Crust and Upper Mantle: Nature, Scaling and Seismic Properties*, pp. 207–236, Kluwer Acad., Norwell, Mass.

Melosh, H. J. (1996), Dynamical weakening of faults by acoustic fluidization, *Nature*, *379*, 601–606.

Mikumo, T., and T. Miyatake (1978), Dynamical rupture process on a three-dimensional fault with non-uniform frictions and near-field seismic waves, *Geophys. J. R. Astron. Soc.*, *54*(2), 417–438.

Mikumo, T., K. B. Olsen, E. Fukuyama, and Y. Yagi (2003), Stress-breakdown time and slip-weakening distance inferred from slip-velocity functions on earthquake faults, *Bull. Seismol. Soc. Am.*, *93*(1), 264–282.

Nielsen, S. B., and L. Knopoff (1998), The equivalent strength of geometrical barriers to earthquakes, *J. Geophys. Res.*, *103*(B5), 9953–9965, doi:10.1029/97JB03293.

Nielsen, S. B., J. M. Carlson, and K. B. Olsen (2000), Influence of friction and fault geometry on earthquake rupture, *J. Geophys. Res.*, *105*(B3), 6069–6088.

Oglesby, D. D., and S. M. Day (2002), Stochastic fault stress: Implications for fault dynamics and ground motion, *Bull. Seismol. Soc. Am.*, *92*(8), 3006–3021, doi:10.1785/0120010249.

Oglesby, D. D., R. J. Archuleta, and S. B. Nielsen (1998), Earthquakes on dipping faults: The effect of broken symmetry, *Science*, *280*(5366), 1055–1059.

Ohnaka, M. (2003), A constitutive scaling law and a unified comprehension for frictional slip failure, shear fracture of intact rock, and earthquake rupture, *J. Geophys. Res.*, *108*(B2), 2080, doi:10.1029/2000JB000123.

Okubo, P. G. (1989), Dynamic rupture modeling with laboratory-derived constitutive relations, *J. Geophys. Res.*, *94*(B9), 12,321–12,335.

Oppenheimer, D. H. (1990), Aftershock slip behavior of the 1989 Loma Prieta, California earthquake, *Geophys. Res. Lett.*, *17*(8), 1199–1202.

Papagerogiou, A. S., and K. Aki (1983), A specific barrier model for the quantitative description of inhomogeneous faulting and the prediction of strong ground motion, II, Applications of the model, *Bull. Seismol. Soc. Am.*, *73*(4), 953–978.

Peyrat, S., K. Olsen, and R. Madariaga (2001), Dynamic modeling of the 1992 Landers earthquake, *J. Geophys. Res.*, *106*(B11), 26467–26482, doi:10.1029/2001JB000205.

Peyrat, S., K. B. Olsen, and R. Madariaga (2004), Which dynamic rupture parameters can be estimated from strong ground motion and geodetic data?, *Pure Appl. Geophys.*, *161*(11–12), 2155–2169, doi:10.1007/s00024-004-2555-9.

Rice, J. R. (1993), Spatiotemporal complexity of slip on a fault, *J. Geophys. Res.*, *98*(B6), 9885–9907.

Rice, J. R. (2006), Heating and weakening of faults during earthquake slip, *J. Geophys. Res.*, *111*, B05311, doi:10.1029/2005JB004006.

Rivera, L., and H. Kanamori (2002), Spatial heterogeneity of tectonic stress and friction in the crust, *Geophys. Res. Lett.*, *29*(6), 1088, doi:10.1029/2001GL013803.

Saucier, F., E. Humphreys, and R. Weldon (1992), Stress near geometrically complex strike-slip faults: Application to the San Andreas fault at Cajon Pass, southern California, *J. Geophys. Res.*, *97*(B4), 5081–5094.

Segall, P., and D. D. Pollard (1980), Mechanics of discontinuous faults, *J. Geophys. Res.*, *85*(B8), 4337–4350.

Shaw, B. E. (1995), Frictional weakening and slip complexity in earthquake faults, *J. Geophys. Res.*, *100*(B9), 18,239–18,251.

Shaw, B. E. (1997), Model quakes in the two-dimensional wave equation, *J. Geophys. Res.*, *102*(B12), 27,367–27,377.

Smith, D. E. (2006), A new paradigm for interpreting stress inversions from focal mechanisms: How 3d stress heterogeneity biases the inversions toward the stress rate, Ph.D. thesis, Calif. Inst. of Technol., Pasadena, Calif.

Somerville, P. G., K. Irikura, R. Graves, S. Sawada, D. Wald, N. Abrahamson, Y. Iwasaki, T. Kagawa, N. Smith, and A. Kowada (1999), Characterizing crustal earthquake slip models for the prediction of strong ground motion, *Seismol. Res. Lett.*, *70*(1), 199–222.

Tinti, E., P. Spudich, and M. Cocco (2005), Earthquake fracture energy inferred from kinematic rupture models on extended faults, *J. Geophys. Res.*, *110*, B12303, doi:10.1029/2005JB003644.

Tse, S. T., and J. R. Rice (1986), Crustal earthquake instability in relation to the depth variation of frictional slip properties, *J. Geophys. Res.*, *91*(B9), 9452–9472.

Turcotte, D. L., and B. D. Malamud (2002), Earthquakes as a Complex System, in *International Handbook of Earthquake and Engineering Seismology*, pp. 209–227, Academic, New York.

Tworzydlo, W. W., and O. N. Hamzeh (1997), On the importance of normal vibrations in modeling of stick slip in rock sliding, *J. Geophys. Res.*, *10*(B7), 15,091–15,103.

Wang, K., J. He, H. Dragets, and T. S. James (2001), Three-dimensional viscoelastic interseismic deformation model for the Cascadia subduction zone, *Earth Planets Space*, *53*, 295–306.

Yoshioka, S., and H. Suzuki (1999), Effects of three-dimensional inhomogeneous viscoelastic structures on postseismic surface deformations associated with the Great 1946 Nankaido earthquake, *Pure Appl. Geophys.*, *154*(2), 307–328.

Zhang, W., T. Iwata, K. Irikura, H. Sekiguchi, and M. Bouchon (2003), Heterogeneous distribution of the dynamic source parameters of the 1999 Chi-Chi, Taiwan, earthquake, *J. Geophys. Res.*, *108*(B5), 2232, doi:10.1029/2002JB001889.

B. T. Aagaard, U.S. Geological Survey, 345 Middlefield Road, MS-977, Menlo Park, CA 94025, USA. (baagaard@usgs.gov)

T. H. Heaton, California Institute of Technology, Mail Stop 252-21, Pasadena, CA 91125, USA. (heaton@caltech.edu)